http://www.jmaterenvironsci.com/

Dialysis-free extraction and characterization of cellulose crystals from almond (*Prunus dulcis*) shells

Najeh Maaloul[1], Rim Ben Arfi[1], Manuel Rendueles[2], Achraf Ghorbal[1,3*], Mario Diaz[2]

[1] *Research Unit UR11ES80, National Engineering School of Gabes, University of Gabes, Avenue Omar Ibn El Khattab 6029 Gabes, Tunisia*

[2] *Department of Chemical Engineering and Environmental Technology, University of Oviedo, Calle San Francisco, 33003 Oviedo, Asturias, Spain*

[3] *Higher Institute of Applied Sciences and Technology of Gabes, University of Gabes, Avenue Omar Ibn El Khattab 6029 Gabes, Tunisia*

Abstract

Pure cellulose crystals (CCs) have been successfully extracted from Tunisian almond shells using a combination of chemical treatments, such as alkaline treatment, bleaching, and sulfuric acid hydrolysis. The hydrolysis products of CCs without further dialysis have been thoroughly characterized. In this work, the chemical analysis of the raw materials revealed interesting levels of α-Cellulose content (29.9 wt%) and lignin content (30.1 wt%). Transmission electron microscopy showed that the sulfuric acid hydrolysis effectively isolated cellulose crystals at the nanometer scale. X-ray diffraction measurements and FTIR spectroscopy analysis confirmed that the isolated crystals are highly crystalline (67.50%) with a cellulose Iβ polymorphic form. The undialyzed CCs showed an apparent crystallite size about 5.66 nm. Thermogravimetric analysis demonstrated that the char yield of CCs, up to 630 °C, was higher than the untreated and pre-treated samples (showing a flame retardant behavior). This work confirms the great potential of undialyzed cellulose crystals for high-end applications.

1. Introduction

In recent years, biodegradable polymers from renewable resources, particularly wastes generated by agriculture, have attracted great attention for a sustainable development and environmental conservation. In this context, the use of biomass residues as feedstock for the production of energy and polymeric materials has been the object of intensive academic and industrial research [1,2]. Indeed, the reuse of agriculture wastes allows a significant diminution of their accumulated volume in the environment and the limitation of the raw materials extraction. Thus, an efficient reuse of these wastes is of great importance, not only as a positive contribution to a healthy ecosystem but also as a source of value-added products [3,4].

Agriculture is an important sector of the Tunisian economy and almond shell is a relatively abundant lignocellulosic agricultural by-product, in Tunisia, with a production of about 70000 tons in 2012 (FAO STAT data, 2012) but it is not much valorized. Currently, the main focus of the Tunisian almond industry is the seed and related foodstuffs and consequently the other fruit parts (shells and hulls) are considered agricultural residues. The use of these crop residues in industrial processes for the generation of value-added products could help in agro-industry diversification by providing a new market for agro-wastes. Like most biomass residues, the almond shell is a biodegradable material composed of cellulose, hemicelluloses and lignin.

The increasing concerns over the effects of deforestation, the rapid depletion of petroleum resources and new environmental regulations have encouraged and accelerated the search for new biopolymers, including cellulose which is the most abundant renewable polymer available on the earth. Indeed, cellulose is produced by nature at an annual rate of 10^{10} - 10^{11} tons and its consumption is continuously increasing even in countries where wood resources are very limited [5]. Therefore, the isolation and further analysis of the characteristics of almond shell cellulose is necessary and relevant for its exploitation and for a potential efficient comparison with others agro-wastes resources. Indeed, researchers have isolated cellulose fibers and crystals from various agro-wastes sources such as tomato peels [6], banana rachis and peels [7-8], pineapple leaf [9], curaua fibers [10] and palmyra palm fruits [11].

The aim of the present work is to process almond shells with a chemical treatment and characterize them in order to evaluate their suitability for the production of undialyzed natural polymers, after an alkali and bleaching treatment for the cellulose isolation. Moreover, an acid hydrolysis was carried out in order to degrade the cellulose amorphous part by keeping the crystalline part. After the acid hydrolysis process, the cellulose crystals are always isolated from the waste hydrolysate by centrifugation and dialysis to remove the soluble sugars and residual acids. However, this dialysis process is time and water consuming [12].

If there exist a significant number of literature on almond shells lignin [13-14] and bio-oil extractions [15-16], there is obviously a lack of research efforts towards the cellulose extraction from this agro-waste. To the best of our knowledge, this is the first time that a paper is entirely dedicated to the extraction and the characterization of undialyzed almond shells cellulose. The morphology, crystallinity and thermal stability of the untreated, alkali treated and bleached and finally the acid hydrolyzed almond shells were investigated with the aim to open up new possibilities of dialysis-free processes and the large scale exploitation of undialyzed cellulose crystals.

2. Materials and methods

2.1. *Materials*

Almond shells were supplied by a local farmer and originated from almond trees (Prunus dulcis) cultivated in the region of Sfax (Tunisia). Tunisian almond shells were used in this work as an original source of cellulose. Sodium hydroxide (POCh SA, ≥98.8%), sulfuric acid (Sigma Aldrich, 95-98%), chloroform (LOBA Chemie, ≥99%), absolute ethanol (VWR-prolabo, ≥99.9%), sodium hypochlorite solution (Sigma Aldrich, 10-15%), acetic acid (Chem-Lab, ≥99.8%), sodium chloride (LABOSI, ≥99.9%) and hydrochloric acid (Chem-Lab, ≥37%) were used without further purification.

2.2. *Pre-treatment of almond shell*

Before the extraction of cellulose, dried almond shell was milled and screened to select the fraction of the particles that were below 60 mesh. The crushed plants fibers were dewaxed with a mixture of chloroform and absolute ethanol (2:1 ratio, v:v) under a mechanical stirring for 24h. Then, the fibers were washed with distilled water until filtrate pH was neutral and dried. Dried product was treated in 4 wt% NaOH solutions at 80-90 °C for 2h to remove hemicelluloses with residual starch and pectin. This alkali treatment was conducted two times, and after each treatment, the fibers were filtered and washed with distilled water to remove the alkali-soluble components. Lignin in the fibers plants was removed by a sodium hypochlorite solution 2.5 wt% at 70 °C for 1h under mechanical stirring and was repeating two times. The bleached fibers were subsequently filtered, washed with distilled water, and air dried. Bleaching treatment was used to facilitate the removal of the majority of the residual lignin content.

2.3. *Sulfuric acid hydrolysis*

Cellulose crystals were prepared by sulfuric acid hydrolysis according to the literature methods [17-18]. The concentration of the acid solution used to immerse the pre-treated cellulose fibers was 40 wt%. The ratios of pre-treated cellulose fibers to the acid solution were 0.05 g/mL. The reaction mixture was maintained at 60 °C. The hydrolysis time in this study was fixed at 45 min, which was found to be the optimum time. Subsequently, large amounts of ice were added to the reaction beaker to stop the hydrolysis. Then, the resulting mixture was filtered and washed with distilled water until filtrate pH was neutral. The suspension of CCs was vacuum-dried at 40°C, cooled in a desiccator, weighted until constant weight achieved, and stored at room temperature for analysis.

2.4. *Determination of fibers composition*

The chemical composition of the Tunisian almond shell was determined according to the American Society for Testing and Materials (ASTM) and the Technical Association of Pulp and Paper Industry (TAPPI) methods. The extractives were removed with an ethanol-toluene mixture according to the ASTM D1107-96 standard method [19]. The holocellulose (α-cellulose + hemicellulose) content was determined according to TAPPI T19 m-54. The α-Cellulose was removed from holocellulose by alkali extraction according to TAPPI T203 om-88. The lignin content of almond shell fibers was determined by a reaction with sulfuric acid according to the TAPPI T222 om-88 standard method. The ash content was measured by considering the percentage difference between the initial weight of the dried fiber of the sample and that after calcination for 8h up to 600 °C according to ASTM D1102-84 [20]. Analyses were performed in triplicate.

2.5. Electron microscopy

Before electron microscopy characterization, untreated and pre-treated fibers were dried in an oven at 40 °C for 24 hours. However, the acid hydrolyzed samples were freeze dried at -70 °C and 0.1 mbar in a Telstar Cryodos freeze-drier to obtain CCs in the powder form.

2.5.1. Scanning electron microscopy

Dry samples were fractured and torn with a blade and fragments were mounted on aluminum SEM stubs, and coated with gold in a Sputtering Balzers SCD 004. Scanning electron microscope (JEOL JSM 6610) was used to study the morphology of the untreated almond shells, the pre-treated fibers, and the extracted cellulose. The acceleration voltage was set at 20 kV.

2.5.2. Transmission electron microscopy

The morphology of the cellulose crystals was collected using Transmission electron microscope (JEOL 2000 EX II) at 120 kV acceleration voltage. A drop of a dilute CCs suspension was deposited on a carbon coated and allowed to dry at room temperature before the TEM observation. The morphology of CCs was analyzed by Digital Micrograph software.

2.6. Attenuated total reflection Fourier transform infrared spectroscopy

Fourier transform infrared spectroscopy (FTIR) measurements were performed using a Spectrum Two PerkinElmer spectrometer, in the attenuated total reflection (ATR) mode, with a highly sensitive deuterated triglycine sulfate (DTGS) detector. The reference (background) spectra using a blank ATR crystal were recorded before scanning each sample. The measurements were carried out at room temperature. The samples were scanned 10 times in the range of 450-4000 cm^{-1}, with a 1 cm^{-1} spectral resolution.

2.7. X-ray diffraction

The X-ray diffraction spectra of the almond shells at different stages of treatment were recorded on a Philips X'Pert X-ray diffractometer. The generator was operated at a voltage of 45 kV and a current of 40 mA; the target was Cu. The diffraction data of the samples were collected over an angular range from 10 to 30° (2θ), with a scanning speed of $0.06°(2\theta)$/min.

The crystallinity index (Ic) of the samples was quantitatively estimated from the diffraction intensity data using the method of Segal [21]. The crystallinity index was obtained by means of Eq. 1

$$I_c = (I_{002} - I_{am})/I_{002} \times 100 \qquad\qquad\qquad \text{Eq.1}$$

where I_{002} peak is the maximum intensity of the (002) lattice diffraction and I_{am} is the intensity attributed to the amorphous part of the sample. The diffraction peak for the plane (002) is located at a diffraction angle around $2\theta = 22°$ and the intensity attributed to the amorphous part is measured as the lowest intensity at a diffraction angle around $2\theta = 18°$. All analyses were at least duplicated.

There is a relation between the size of the crystals and the pattern that would be recorded by the diffractometer. That relationship is defined by the widely used Scherrer's equation Eq. (2) given by [22-24]

$$D_{hkl} = K\lambda/(\beta \cos\theta) \qquad\qquad\qquad \text{Eq.2}$$

where D_{hkl} is the crystallite dimension in the direction normal to the hkl lattice planes, λ is the wavelength of the incident X-ray (1.54060 Å), θ the Bragg angle corresponding to the (002) plane, β the full-width at half maximum (FWHM) of the X-ray peak corresponding to the (002) plane, and K is a constant that depends on the crystal shape usually considered 0.9.

2.8. Thermogravimetry (TGA) and differential thermogravimetry (DTG)

Thermogravimetric measurements (TGA/DTG) of untreated almond shells, alkali treated and bleached fibers and cellulose crystals were performed by a Mettler Toledo TGA / SDTA851 instrument. The samples were heated from 25 to 900 °C at a heating rate of 20 °C/min under a nitrogen atmosphere with a gas flow of 50 mL/min. The amount of sample used for each measurement was about 18 mg.

2.9. *Conductometric titration*

The acid group content of cellulose crystals (-O-SO$_3^-$) was determined by conductometric titration. Briefly, 100 mg of CCs was suspended in 50 ml of 0.01 mM NaCl and poured into a 100 ml three-necked round-bottomed flask. Then the mixture was stirred continuously for 10 min. The suspension was titrated using 0.002 M sodium hydroxide. Finally, the amount of sulfate ester groups (-O-SO$_3^-$) on CCs was calculated by Eq.3 given by [25]

$$X = CV/m \times 10^6 \qquad\qquad \text{Eq.3}$$

Where X is the total acid group content (μmol/g), C is the NaOH concentration (mol/L), V is the amount of NaOH (L) consumed corresponding to the plateau region and m (g) is the weight of the CCs in the water suspensions.

3. Results and discussion

3.1. *Chemical composition*

Up to our knowledge, the only partial composition data on Tunisian almond shells is given in Grioui et al. study [15]. α-Cellulose content (29.9 ± 0.7 wt%) is comparable with the values reported in the literature for Tunisian (26 wt%) and Iranian (29.1 wt%) almond shells and lower compared to Spanish (37.4 wt%) and Turkish (50.7 wt%) almond shells. The hemicellulose content (25.1 ± 0.7 wt%) is lower than the range (28.7 - 35.2 wt%) reported in the literature for other sorts of almond shells. The lignin content (30.1 ± 0.5 wt%) is higher than the Spanish (27.5 wt%) and the Turkish (20.4 wt%) almond shells. The ash content of characterized almond shells was found to be around (3.4 ± 0.1 wt%). This value is equal to the ash content of the Iranian (3.4 wt%) almond shells, comparable to values reported for Tunisian (2.7 wt%) and Turkish (3.3 wt%) raw materials and much higher than the Spanish (0.5 wt%) one. The extractives content in this study (11.8 ± 0.2 wt%) is higher compared with previous studies on Iranian (2.8 wt%) and Spanish (3.9 wt%) almond shells [26-28].

A comparison of the chemical composition of almond shell fibers, on the dry basis, with some important natural fibers, almond shells from different origins and agricultural residues is presented in Table 1. It is evident that plants like sugarcane bagasse [29], alfa [30], jute [31], capim dourado [32] and sisal [33] have higher cellulose content compared to Tunisian almond shell. However, its abundance can be a valid basis for exploitation as a raw material for paperboard production and the development of eco-composites.

Table 1: Comparative chemical composition (wt%) of Tunisian almond shell fibers with some other natural fibers.

Raw material	α-Cellulose	Hemicellulose	Lignin	Ash	Extractives	References
Tunisian almond shell	29.9 ± 0.7	25.1 ± 0.7	30.1 ± 0.5	3.4 ± 0.1	11.8 ± 0.2	This study
	26	29 − 30	28 − 33	2.71	–	[15]
Spanish almond shell	37.4	31.2	27.5	0.55	3.9	[26]
Turkish almond shell	50.7	28.7	20.4	3.3	–	[16]
Iranian almond shell	29.1	35.2	32.7	3.4	2.8	[27]
Sugarcane bagasse	54.3 − 55.2	16.8 − 29.7	24.3 − 25.3	1.1	0.7 − 3.5	[29]
Alfa	46 ± 3	24 ± 2	20 ± 2	7.2 ± 1.0	−	[30]
Jute	60	22.1	15.9	1	−	[31]
Capim Dourado	66.5 − 67.8	22.5 − 24	6 − 7	1−1.2	0.7 − 0.8	[32]
Sisal	65 ± 1	20 ± 1	12 ± 1	1 ± 0.1	−	[33]

3.2. *Morphological analysis*

The color of the fibers changed from brown to light yellow after alkali treatment and bleaching and became white after sulfuric acid hydrolysis. Scanning electron microscopic analyzes of treated and untreated almond shell fibers were carried out to assess their surface morphology at the micron and submicron level. Fig. 1 shows the SEM micrographs of a raw ground almond shell, pretreated and acid hydrolyzed materials. The SEM micrograph of the raw material fibers (Fig. 1(a)) revealed an irregular structure and some residues from the grinding procedure. Moreover, these micrographs evidenced the size reduction of fibers aggregates that takes place during the bleaching process (Fig. 1(b)). Indeed, the cementing materials, i.e. the lignin and hemicelluloses, present in the fibers get dissolved out more predominantly during the bleaching process [34]. The SEM image of the acid hydrolyzed fibers (Fig. 1(c)) evidenced the size reduction and the morphological changes of treated materials, showing as a consequence a gradual removal of amorphous components, and the permanence of the crystal cellulosic portion.

The TEM images of isolated cellulose crystals are shown in Fig. 2. It can be seen that the undialyzed cellulose crystals are spherical and at the nanosize level, i.e. diameter about 200 nm. The diameters of almond shell CCs were similar to synthesized nanospherical whiskers [35] and the size range of cylinder-like and needle-like structures derived from other sources(using dialysis process) such as wheat straw fibers (200nm –1 mm) [36] and coconut fibers (128 nm – 208 nm) [37], respectively.
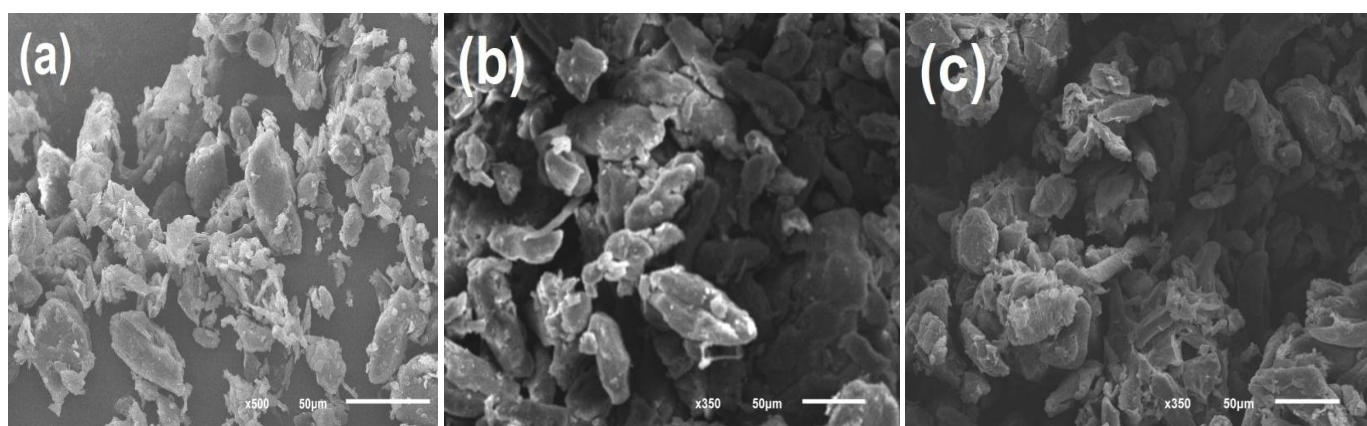
Figure 1: SEM photomicrographs at different stages of the cellulose extraction process; (a) ground almond shells; (b) alkali treated and bleached fibers; (c) acid hydrolyzed fibers.
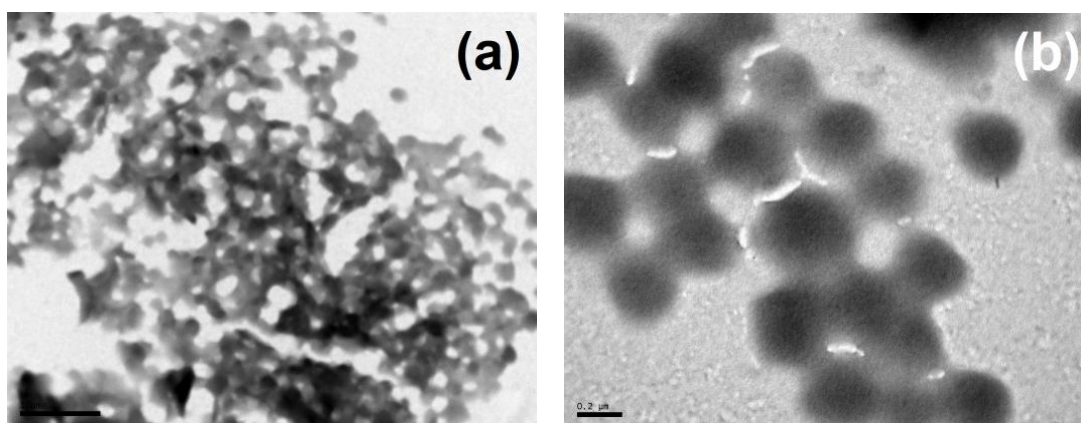
Figure 2: TEM photomicrographs of undialyzed cellulose crystals extracted from almond shells. (a) Large scale image of isolated CCs (scale bar : 1 μm); (b) Isolated CCs with a sphere-like shape (scale bar : 200 nm).

3.3. *FTIR spectroscopy analysis*

FTIR-ATR spectroscopy analyzes of untreated, alkali treated and bleached and acid hydrolyzed almond shell revealed compositional changes in the structure of fibers during the chemical treatments. Fig. 3 depicts the FTIR-ATR spectra of the untreated, pretreated and hydrolyzed almond shell.
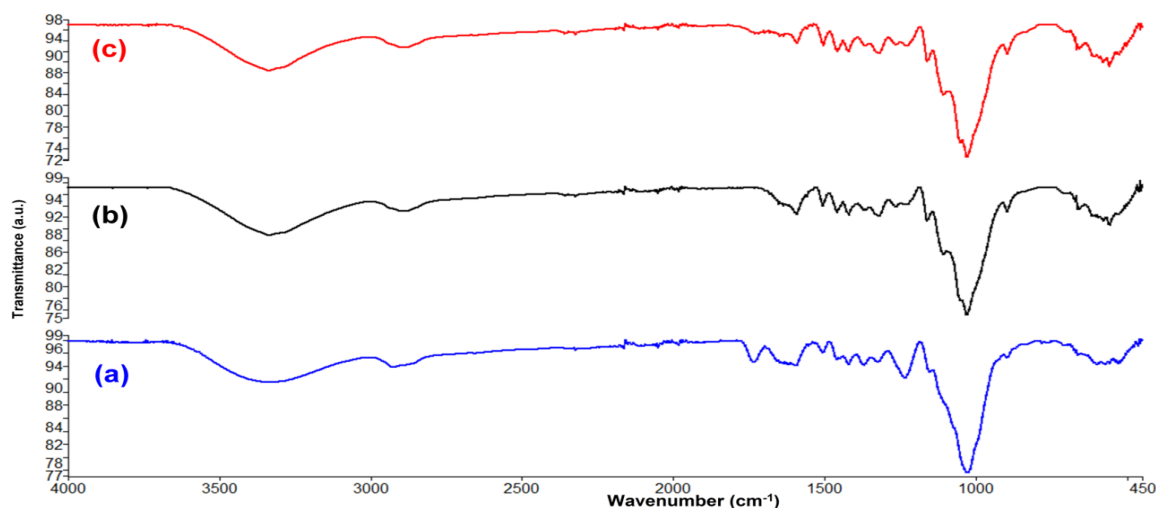
Figure 3: ATR-FTIR spectra of (a) untreated almond shell fibers; (b) alkali treated and bleached fibers; (c) undialyzed cellulose crystals.

The broadened band of the OH-stretching at around 3650–3000 cm^{-1} is observed in all spectra. The signal at 2900 cm^{-1} was due to the aliphatic saturated C-H stretching vibration in cellulose and hemicelluloses. The vibration at 2850 cm^{-1} originating from C-H stretching in lignin and waxes was highly attenuated after the different chemical treatments. Moreover, FTIR-ATR spectra show that bleaching and NaOH treatments removed most of the lignin, as seen by the reduction of the intensity of peaks of aromatic ring vibrations at 1594 cm^{-1} and 1509 cm^{-1}, C-H deformations at 1460 cm^{-1} and guaiacyl ring breathing with stretching C=O at 1235 cm^{-1} [38-39].

The signal at 1732 cm^{-1}, that represents vibrations of acetyl and uronic ester groups of hemicelluloses or ester linkage of carboxylic group of the ferulic and p-coumaric acids of lignin, was significantly reduced [40].

In all spectra, the band near to 1045 cm^{-1} (C-O-C stretching) is due to the presence of xylans associated with hemicelluloses. This suggests that xyloglucans are strongly bound to cellulose microfibrils. Interestingly, drastic change in intensity at 1105 cm^{-1} for the sample treated with NaOH was observed. This can be associated with changes in the hydrogen bonding system, and it possibly indicates the transition from cellulose I to cellulose II. The C–O–C pyranose ring skeletal vibration gives a very intense band at 1024 cm^{-1} evidencing a high cellulose content [41].

Moreover, the small sharp band at 893 cm^{-1} in the FTIR spectra of extracted cellulose samples was typical of the structure of cellulose and represented glycosidic C–H deformation, with a ring vibration contribution from O–H bending [42]. These features evidenced β-glycosidic linkages between the anhydroglucose units in cellulose. Indeed, natural cellulose consists of a number of polymorphs; specifically, cellulose Iα and Iβ. Following the assignment of Sugiyama [43], the peaks near 3240 cm^{-1} and 750 cm^{-1} are assigned to the Iα phase whereas those near 3270 cm^{-1} and 710 cm^{-1} correspond to the Iβ phase. Thus, the marked bands at 3270 cm^{-1} and 710 cm^{-1} in Fig. 4 clearly show that the extracted cellulose is particularly rich in cellulose Iβ type polymorph.

3.4. *X-ray diffraction measurements*
The influence of the chemical treatment on the nature of the resulting materials was investigated. Fig. 5 shows the XRD patterns for almond shells at different stages of treatment. These patterns are typical of semi-crystalline materials with an amorphous broad hump and crystalline peaks [44]. All the X-ray diffractograms show that there is a predominance of cellulose type I verified by the presence of the well-defined (110) and (002) peaks at 2θ = 16° and 22.6°, respectively. The peak at 2θ = 26.5° present in all the spectra is related to the sample holder. The diffraction peaks at 2θ = 14.93° (100) and 24.37° (004), observed in diffractograms of the raw materials, are often assigned to the phase of whewellite (Ca oxalate monohydrate, $CaC_2O_4.H_2O$ - JCPDF 20-0231) [45-46]. This mineral crystal was removed from the raw materials by the alkali and bleaching treatments. The X-ray diffraction pattern revealed that the untreated almond shell contained a large amorphous portion. Indeed, as shown in Table 2, the crystallinity index (Ic) of the untreated, the alkali treated and bleached, and the acid hydrolyzed almond shell calculated by Eq.1 was 46.82%, 65.69%, and 67.50%, respectively. These results clearly demonstrate that the crystallinity of the treated materials increases significantly during the chemical extraction particularly after the alkali and the bleaching treatments.
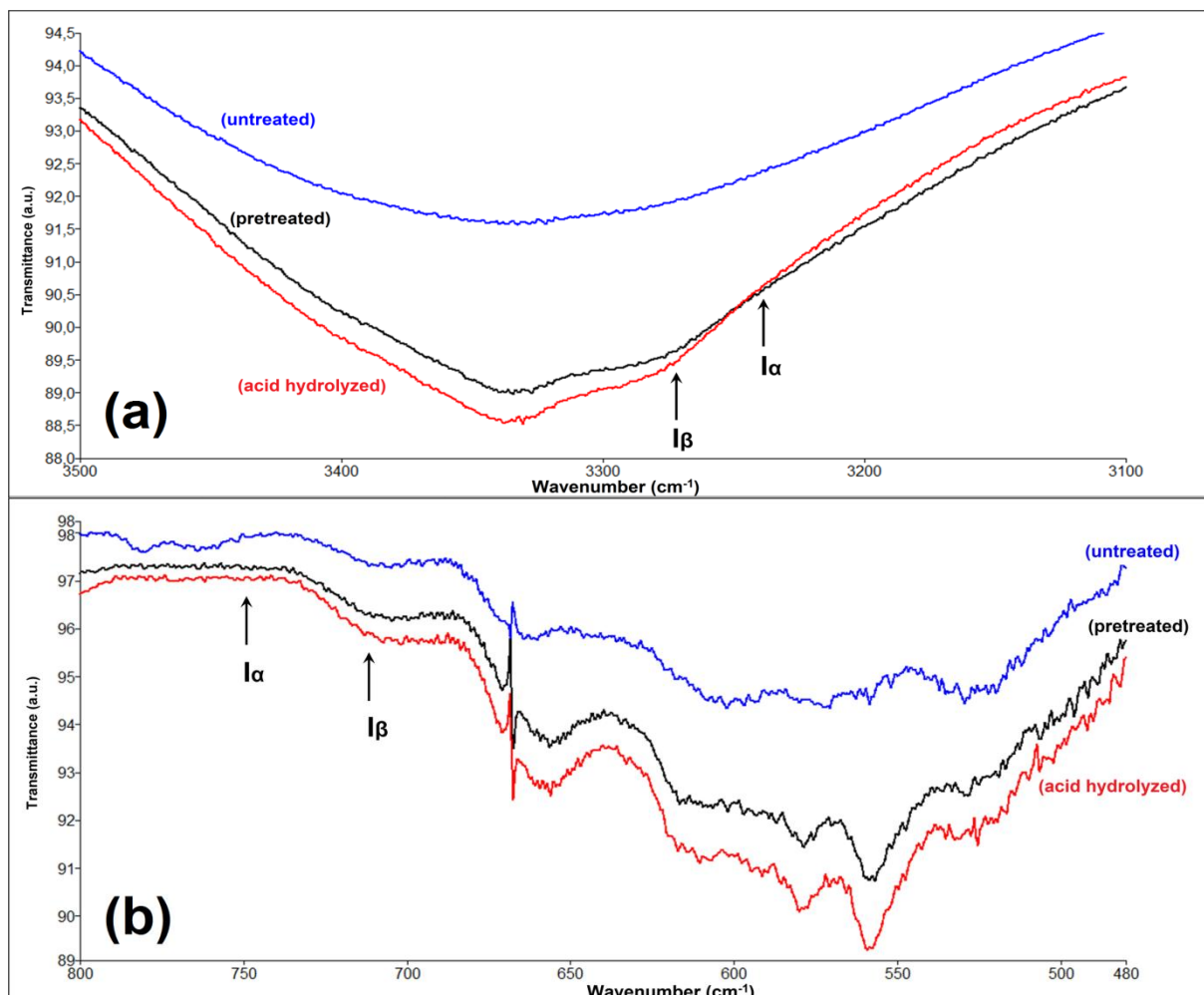
Figure 4: ATR-FTIR spectra at different stages of cellulose extraction from almond shells. (a) Spectra region from 3100 to 3500 cm^{-1}. (b) Spectra region from 480 to 800 cm^{-1}.
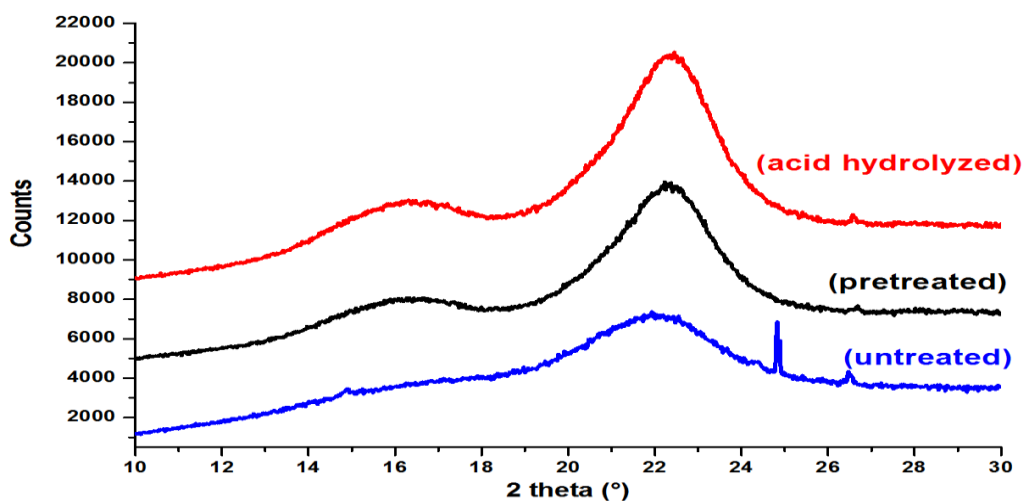
Figure 5: XRD patterns of untreated almond shell fibers, alkali treated and bleached fibers and undialyzed cellulose crystals.

Indeed, the removal of non-cellulosic components (hemicelluloses and lignin), which are located in the amorphous regions, lead to more organized cellulose chains. It is important to note that the highest Ic value (67.50%) corresponds to the hydrolyzed materials, which displayed the highest and the sharpest peak at $2\theta =$ 22.4°. This observation usually reveals better defined crystalline domains, which is in concordance with the

morphological analysis. In fact, the increase of the crystallinity index value under the sulfuric acid hydrolysis effect is often indicative of the dissolution of amorphous cellulosic domains. Indeed, during the process of hydrolysis, the hydronium ions could penetrate into the amorphous regions of cellulose and allow the cleavage of glycosidic bonds by acid hydrolysis [47]. This finally leads to the release of the individual crystallites. This increase in the crystallinity index often leads to the cellulose stiffness and rigidity increase [48]. Thus, one can say that acid hydrolyzed almond shells could provide a remarkable reinforcing potential and a great potential in high-end applications. However, the presence of sulfate groups from sulfuric acid hydrolysis in the outer surface of the crystals has been proved to decrease the material thermal stability, which is probably a key factor when intending to use CCs as reinforcement [49]. It is important to note that the 67.50% crystallinity value of the acid hydrolyzed and undialyzedTunisian almond shells is higher than wastepaper (65.8%) [50], multistep-treated (54%) or hydrothermally-treated (58%) mandarin peel waste [51], extracted cellulose microfibrils from coconut palm leaf sheath (47.7%) [1], rice husks cellulose crystals (59%) [48] and barley husks cellulose crystals (66%) [52]. As a consequence, one can consider the Tunisian almond shells as a competitive crystalline cellulose.

The apparent crystallite size was determined for the various samples and the results are summarized in Table 2. The apparent crystallite size, unlike the crystallinity index, was found to decrease after each treatment step. Indeed, the apparent crystallite size of the untreated, the alkali treated and bleached, and the acid hydrolyzed almond shell was 17.9 nm, 11.94 nm, and 5.66 nm, respectively. This clearly shows that chemical treatments resulted in the decrease of the crystallite size. The first reduction of the crystallite size may be mainly due to the coupling effect of the penetration of alkali solution in the crystalline regions and the peeling off of chains from crystallites [53]. The second reduction of the crystallite size is directly related to the cellulose degradation under the acid hydrolysis treatment. This result is contradicted by the reports of other groups where the crystallite size of nanocrystals increased compared to the corresponding starting material [54-55]. The increase of the crystallite size was ascribed to the good alignment and the low sulfur contents of the rod-like nanocelluloses. However, the extracted almond shell crystals have relatively higher surface charges (The sulfate ester groups content was calculated to be 77.4 $\mu mol.g^{-1}$), which probably prevent the crystals close packing, the formation of hydrogen bonds between CCs, and consequently the increase of the crystallite size.

Table 2: Crystallinity index (Ic) and apparent crystallite sizes (D_{hkl}) of untreated, pre-treated, and acid hydrolyzed almond shells

Material	$2\theta°$ (am)	$2\theta°$ (002)	Ic (%)	D_{hkl} (nm)
untreated	18.2	22.0	46.82	17.90
alkali treated and bleached	18.1	22.2	65.69	11.94
acid hydrolyzed	18.1	22.4	67.50	5.66

3.5. *Thermogravimetric analysis*

The thermostability of the studied samples is a key factor in the evaluation of their potential use in composites because the processing temperature exceeds generally 200°C. Thermal stability of the untreated, the alkali treated and bleached, and the acid hydrolyzed almond shell were investigated by TGA and DTG in an inert atmosphere (nitrogen) are shown in Fig. 6(a-b). The thermal decomposition of the untreated, the alkali treated and bleached and the acid hydrolyzed almond shell occurred in different pyrolysis processes. The complexity of this degradation results from a large number of steps of parallel and consecutive reactions. Indeed, all samples had a small weight loss in the low temperature range (below 120 °C for the acid hydrolyzed sample and 150 °C for the untreated and the alkali treated and bleached samples). The initial change is ascribed to the vaporization of absorbed water. In the high temperature range (above 150 °C), the degradation behaviors of the three samples were different.

For the untreated sample, the degradation occurs above 220 °C until approximately 410 °C and showed two pyrolysis processes in the DTG curves. The first process occurred between 220 °C and 310 °C, resulted mainly from the depolymerization of hemicelluloses, the broke of the glycosidic linkages of cellulose and the decomposition of some portion of lignin. The second process in the temperature range (310-410 °C) was associated with degradation of cellulose and lignin. The lignin degradation took place above 450 °C [56].

The TGA and DTG curves of the alkali treated and bleached samples showed almost the same thermal curve shapes of the untreated almond shell below 150 °C. However, in the temperature range (220-410 °C), one can

distinguish a narrower and more intense degradation peak showing only one pyrolysis process. Indeed, the disappear of the DTG peak at around 320 °C likely reflects the removal of an important portion of hemicelluloses and lignin after the alkali and bleaching treatments.
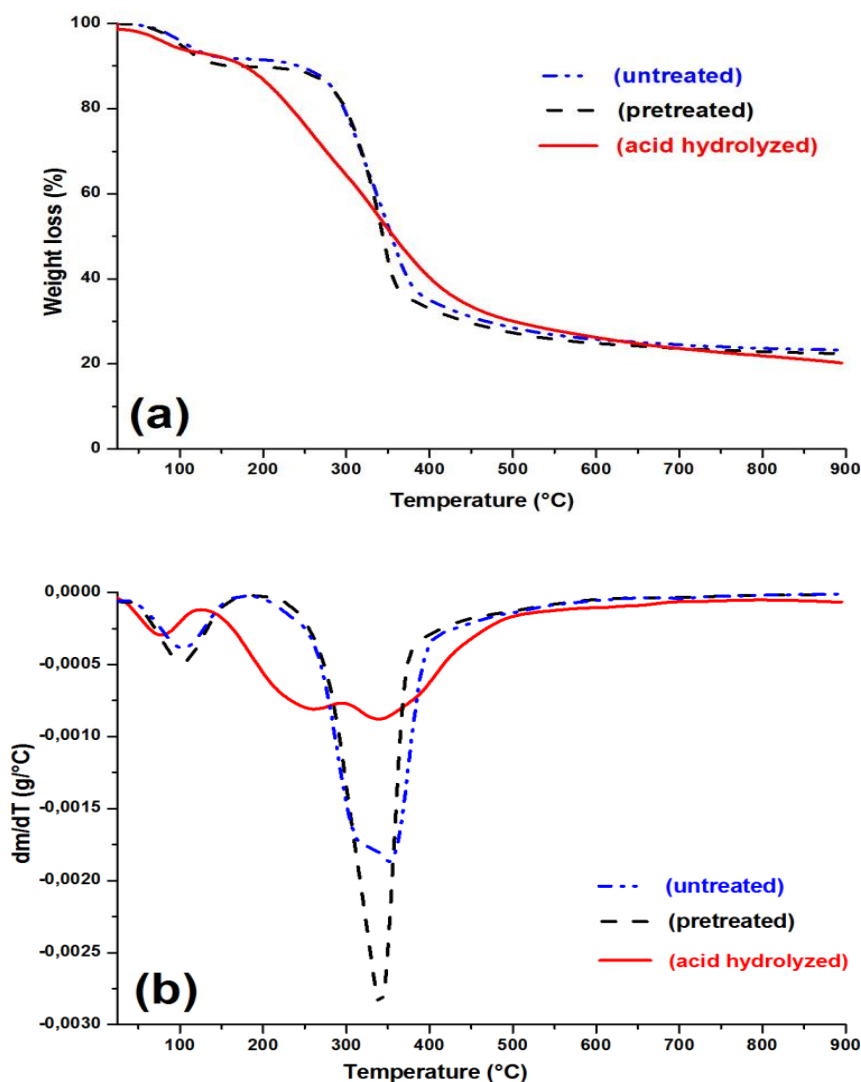
Figure 6: TGA (a) and DTG (b) curves of untreated almond shell fibers, pre-treated fibers and undialyzed cellulose crystals.

On the basis of the TGA and DTG curves of the acid hydrolyzed almond shell, one can say that this sample shows typical thermal behavior of cellulose nanocrystals, as reported in previous studies [57]. This result is in perfect agreement with TEM and XRD characterizations. Kim et al. [58] showed that sulfuric acid treatment leads to a remarkable decrease in thermal stability of nanocellulose. This occurs because the integration of sulfate groups at the outer surface of cellulose chains activate the catalysis of their thermal degradation reactions [17]. It is important to remember that the content of acid sulfate groups in the extracted CCs was calculated to be 77.4 $\mu mol.g^{-1}$. As can be observed in the DTG graph Fig. 6(b), the acid hydrolyzed sample degradation occurred within a distinctly wider temperature range (150–500 °C) than that of alkali treated and bleached samples and showed two well separated and consecutive pyrolysis reactions, suggesting cellulose crystals with different sulfonation degrees.

According to Martins et al. [59], this catalysis could proceed either directly through the acid molecules or indirectly by promoting dehydration reactions. Indeed, the cellulose thermal degradation with acid catalyst was usually hypothesized with two consecutive reactions. Under the catalysis of acid sulfate groups, the dehydration reaction initially took place, at a lower temperature, at cellulose chain units directly containing these groups. The subsequent degradation reaction occurred at the cellulose chains which were in the interior part of the cellulose crystal or not in direct contact with the catalyst.

The TGA results clearly illustrate that the thermal stability of the untreated and the alkali treated and bleached samples was higher than that of the acid hydrolyzed sample. However, the char yield of cellulose crystals, below 630 °C, was higher than that of the other samples. This could be due to the higher amount of free end chains showed by the CCs. In fact, the end chains start decomposition at lower temperatures. Consequently the residual mass fraction of hydrolyzed samples increases. Moreover, this could be caused by the introduction of sulfate groups during hydrolysis which act as a flame retardant by promoting dehydration reactions [60].

Above 630 °C, the char yield of the untreated and alkali treated and bleached samples was higher than that of the acid hydrolyzed sample. This is due to the presence of higher phenyl groups of lignin, particularly in the untreated almond shell. Indeed, the lignin phenyl groups are the most difficult lignocellulosic component groups to decompose and their decomposition extended to the whole temperature range, starting below 200 °C and up to 900 °C, as shown in Fig. 6(a).

Conclusions

In this work, the successful production of spherical cellulose crystals was demonstrated, allowing us to add the almond shell to the list of economically viable cellulose sources. The physical and chemical properties of Tunisian almond shells, pretreated fibers, and extracted CCs were characterized. The results of the α-Cellulose, hemicellulose, lignin and ash content analysis, X-ray diffraction, FTIR-ATR spectroscopy analyzes, conductometric titration and thermogravimetric measurements showed that the undialyzed CCs have a great potential in high-end applications.

Indeed, the (alkali treatment/sodium hypochlorite bleaching/sulfuric acid hydrolysis) process removed lignin and hemicelluloses and led to the extraction of highly crystalline (67.50%) crystals with a cellulose Iβ polymorphic form. The undialyzed CCs of Tunisian almond shell showed a sphere-like shape with a mean diameter of about 200 nm. The sulfate ester groups ($-O-SO_3^-$) content on undialyzed crystals was calculated to be 77.4 µmol.g^{-1}. Owing to their abundance, high crystallinity, dispersibility in polar solvents and biodegradability, CCs serve as promising candidates for the preparation of new composites and biosorbents.

References

1. Uma Maheswari C., Obi Reddy K., Muzenda E., Guduri B.R., Varada Rajulu A., *Biomass and Bioenergy.* 46 (2012) 555.
2. Deepa B., Abraham E., Cordeiro N., Mozetic M., Mathew A.P., Oksman K., Faria M., Thomas S., Pothan L. A., *Cellulose.* 22 (2015) 1075.
3. Eddebbagh M., Abourriche A., Berrada M., Ben Zina M., Bennamara A., *J. Mater. Environ. Sci.* 7 (2016) 2021.
4. Nwosu F.O.; Muzakir, M.M., *J. Mater. Environ. Sci.* 7 (2016) 1663.
5. Hon D.N.S., *Cellulose.* 1 (1994) 1.
6. Jiang F., Hsieh Y.-L., *Carbohydr. Polym.* 122 (2015) 60.
7. Zuluaga R., Putaux J.L., Cruz J., Vélez J., Mondragon I., Gañán P., *Carbohydr. Polym.* 76 (2009) 51.
8. Tibolla H., Maria F., Cecilia F., *LWT Food Sci. Technol.* 59 (2014) 1.
9. Dos Santos R.M., Neto Flauzino W.P., Silvério H.A., Martins D.F., Dantas N.O., Pasquini D., *Ind. Crops Prod.* 50 (2013) 707.
10. Corrêa A.C., de Teixeira E.M., Pessan L.A., Mattoso L.H.C., *Cellulose.* 17 (2010) 1183.
11. Rosa M.F., Medeiros E.S., Malmonge J. A., Gregorski K.S., Wood D.F., Mattoso L.H.C., Glenn G., Orts W.J., Imam S.H. Carbohydr. Polym. 81 (2010) 83.
12. Zhang X., Wu X., Lu C., Zhou Z., *ACS Sustain. Chem. Eng.* 3 (2015) 675.
13. Quesada-Medina J., López-Cremades F.J., Olivares-Carrillo P., *Bioresour. Technol.* 101 (2010) 8252.
14. Gong D., Holtman K.M., Franqui-Espiet D., Orts W.J., Zhao R., *Biomass and Bioenergy.* 35 (2011) 4435.
15. Grioui N., Halouani K., Agblevor F. A., *Energy Sustain. Dev.* 21 (2014) 100.
16. Önal E., Uzun B.B., Pütün A.E., *Energy Convers. Manag.* 78 (2014) 704.
17. Roman M., Winter W.T., *Biomacromolecules.* 5 (2004) 1671.
18. De Morais Teixeira E., Corrêa A.C., Manzoli A., de Lima Leite F., de Ribeiro Oliveira C., Mattoso L.H.C., *Cellulose.* 17 (2010) 595.

19. ASTM D1107 - 96, Standard Test Method for Ethanol-Toluene Solubility of Wood, *ASTM Int.* (2013).
20. ASTM D1102 - 84: Standard Test Method for Ash in Wood. *ASTM Int.* (2013).
21. Segal L., Creely J.J., Martin A. E., Conrad C.M., *Text. Res. J.* 29 (1959) 786.
22. Holzwarth U., Gibson N., *Nat. Nanotechnol.* 6 (2011) 534.
23. Poletto M., Júnior H., Zattera A., *Materials (Basel).* 7 (2014) 6105.
24. Filson P.B., Dawson-Andoh B.E., Schwegler-Berry D., *Green Chem.* 11 (2009) 1808.
25. Zhao Y., Zhang Y., Lindström M.E., Li J. *Carbohydr. Polym.* 117 (2015) 286.
26. González J.F., Ramiro A., González-García C.M., Gañán J., Encinar J.M., Sabio E., Rubiales J., *Ind. Eng. Chem. Res.* 44 (2005) 3003.
27. Pirayesh H., Khazaeian A., *Compos. Part B Eng.* 43 (2012) 1475.
28. Urruzola I., Robles E., Serrano L., Labidi J., *Cellulose.* 21 (2014) 1619.
29. Satyanarayana K.G., Guimarães J.L., Wypych F., *Compos. Part A Appl. Sci. Manuf.* 38 (2007) 1694.
30. Ben Mabrouk A., Kaddami H., Boufi S., Erchiqui F., Dufresne A., Cellulose. 19 (2012) 843.
31. Razera I.A.T., Frollini E., *J. Appl. Polym. Sci.* 91 (2004) 1077.
32. Siqueira G., Abdillahi H., Bras J., Dufresne A., *Cellulose.* 17 (2010) 289.
33. Megiatto J.D., Hoareau W., Gardrat C., Frollini E., Castellan A., *J. Agric. Food Chem.* 55 (2007) 8576.
34. Deepa B., Abraham E., Cherian B.M., Bismarck A., Blaker J.J., Pothan L. A., Leao A.L., de Souza S.F., Kottaisamy M., *Bioresour. Technol.* 102 (2011) 1988.
35. Zhang J., Elder T.J., Pu Y., Ragauskas A.J., *Carbohydr. Polym.* 69 (2007) 607.
36. Rahimi M., Behrooz R., *Int. J. Polym. Mater.* 60 (2011) 529.
37. Do Nascimento D.M., Almeida J.S., Vale M. do S., Leitão R.C., Muniz C.R., de Figueirêdo M.C.B., Morais J.P.S., Rosa M. de F., *Ind. Crops Prod.* (2016). doi:10.1016/j.indcrop.2015.12.078.
38. Pelissari F.M., Sobral P.J.D.A., Menegalli F.C., *Cellulose.* 21 (2014) 417.
39. Strassberger Z., Prinsen P., Van Der Klis F., Van Es D.S., Tanase S., Rothenberg G., *Green Chem.* 17 (2015) 325.
40. Amiralian N., Annamalai P.K., Memmott P., Taran E., Schmidt S., Martin D.J., *RSC Adv.* 5 (2015) 32124.
41. Mohamed M.A., Salleh W.N.W., Jaafar J., Asri S.E.A.M., Ismail A.F., *RSC Adv.* 5 (2015) 29842.
42. Chen Z., Hu T.Q., Jang H.F., Grant E., *Carbohydr. Polym.* 127 (2015) 418.
43. Sugiyama J., Persson J., Chanzy H., *Macromolecules.* 24 (1991) 2461.
44. Silvério H.A., Flauzino Neto W.P., Dantas N.O., Pasquini D., *Ind. Crops Prod.* 44 (2013) 427.
45. Yusenko E. V., Yusenko K. V., Korolkov I. V., Shubin A.A., Kapsargin F.P., Efremov A.A., Yusenko M. V., *Cent. Eur. J. Chem.* 11 (2013) 2107.
46. Bettaieb F., Khiari R., Dufresne A., Mhenni M.F., Putaux J.L., Boufi S., *Ind. Crops Prod.* 72 (2015) 97.
47. Fortunati E., Puglia D., Monti M., Peponi L., Santulli C., Kenny J.M., Torre L., *J. Polym. Environ.* 21 (2013) 319.
48. Johar N., Ahmad I., Dufresne A., *Ind. Crops Prod.* 37 (2012) 93.
49. Tee T.T., Sin L.T., Gobinath R., Bee S.T., Hui D., Rahmat A.R., Kong I., Fang Q., *Compos. Part B Eng.* 47 (2013) 238.
50. Danial W.H., Abdul Majid Z., Mohd Muhid M.N., Triwahyono S., Bakar M.B., Ramli Z., *Carbohydr. Polym.* 118 (2015) 165.
51. Hiasa S., Iwamoto S., Endo T., Edashige Y., *Ind. Crops Prod.* 62 (2014) 280.
52. Espino E., Cakir M., Domenek S., Román-Gutiérrez A.D., Belgacem N., Bras J., *Ind. Crops Prod.* 62 (2014) 552.
53. Fink H.P., Hofmann D., Philipp B., *Cellulose.* 2 (1995) 51.
54. Lu P., Hsieh Y.-L., *Carbohydr. Polym.* 87 (2012) 564.
55. Liu Y., Wang H., Yu G., Yu Q., Li B., Mu X., *Carbohydr. Polym.* 110 (2014) 415.
56. Yang H., Yan R., Chen H., Lee D.H., Zheng C., *Fuel.* 86 (2007) 1781.
57. Jiang F., Han S., Hsieh Y.-L., *RSC Adv.* 3 (2013) 12366.
58. Kim D.Y., Nishiyama Y., Wada M., Kuga S., *Cellulose.* 8 (2001) 29.
59. Martins M.A., Teixeira E.M., Corrêa A.C., Ferreira M., Mattoso L.H.C., *J. Mater. Sci.* 46 (2011) 7858.
60. Li S., Li C., Li C., Yan M., Wu Y., Cao J., He S., *Polym. Degrad. Stab.* 98 (2013) 1940.

(2017) ; http://www.jmaterenvironsci.com